doi: 10.4149/gpb_2025015

Knockdown of PLK1 suppresses malignant phenotypes and tumor growth in bladder cancer *via* activating Hippo pathway

Yue Yang[1,*], Yunhan Wang[1,*], Zhou Zheng[2], Hanchao Zhang[1] and Haifeng Hu[1]

[1] *Department of Urology, The Affiliated Hospital and Clinical Medical College of Chengdu University, China*
[2] *Department of Urology, The Traditional Chinese Medicine Hospital of Longquanyi, Chengdu, China*

Abstract. Bladder cancer (BLCA) is a prevalent urological malignancy. We aim to identify novel biomarkers for BLCA and elucidate the specific regulatory mechanisms of polo-like kinase 1 (PLK1). Using differentially expressed genes (DEGs) screened from GSE38264 and GSE130598 datasets, we constructed protein-protein interaction networks to identify hub genes, whose expression was validated using reverse transcription-quantitative polymerase chain reaction. The malignant phenotype of BLCA cells was assessed by Cell Counting Kit-8, 5-ethynyl-2'-deoxyuridine, Transwell, and wound-healing assays. Hematoxylin-eosin and immunohistochemical staining were employed to evaluate BLCA development in mouse xenograft models. The protein expression was detected by Western blot. PLK1, AURKA, AURKB, CDK1, ERBB2, ERBB3, FGFR1, FYN, ABL1, and PRKDC were hub genes with predictive value for BLCA. Among them, PLK1 was selected as a key target of BLCA. PLK1 knockdown inhibited the *via*bility, proliferation, migration, and invasion of BLCA cells. *In vivo*, PLK1 knockdown inhibited tumor growth. Silencing PLK1 activated the Hippo pathway in BLCA cells and tumor tissues. The Hippo pathway inhibitor reversed the inhibitory effects of PLK1 silencing on malignant phenotype of BLCA cells. PLK1 knockdown exerts an inhibitory effect on BLCA *via* activating the Hippo pathway, which presents promising therapeutic strategies for BLCA.

Key words: Bladder cancer — Hub genes — PLK1 — Hippo pathway — Biomarkers

Highlights

- PLK1, AURKB, CDK1, and FYN are novel biomarkers of BLCA.
- Knockdown of PLK1 inhibits BLCA.
- Knockdown of PLK1 activates Hippo pathway to inhibit BLCA.

Introduction

Bladder cancer (BLCA) is among the most prevalent malignancies worldwide, resulting in nearly 170, 000 deaths annually (Jubberg et al. 2023). Exposure to carcinogens in both environmental and occupational settings, notably tobacco, has been identified as a primary risk factor for BLCA (Dyrskjøt et al. 2023). This disease is typically heterogeneous and is classified into two main subtypes: non-muscle-invasive BLCA (NMIBC) and muscle-invasive BLCA (MIBC). The distinction between these subtypes is primarily based on whether the tumor invades the muscular layer of the bladder (Sanli et al. 2017). When detected before muscle invasion, BLCA is typically treatable and can have minimal impact on survival. Muscle-invasive disease may metastasize, primarily to lymph nodes, bones, lungs, and liver, with a median survival period of approxi-

* These authors contributed equally to this work.
Electronic supplementary material. The online version of this article (Doi: 10.4149/gpb_2025015) contains Supplementary material.
Correspondence to: Haifeng Hu, No. 82, Section 2, North Second Ring Road, Jinniu District, Chengdu City, Sichuan Province, 610000, China
E-mail: yyjakejerry@163.com

mately 15 months (Facchini et al. 2020; Tran et al. 2021). Currently, the primary treatment modalities for patients with NMIBC include tumor resection and adjuvant intravesical therapy, whereas those with MIBC may undergo cystectomy and urinary diversion (Compérat et al. 2022; Flaig et al. 2022). However, approximately 50% of patients with MIBC experience recurrence within two years postoperatively, and 10–15% of these patients present with metastases at the time of recurrence diagnosis (Witjes et al. 2021; Lobo et al. 2022). Consequently, identifying potential biomarkers for BLCA is crucial for improving early detection, guiding personalized treatment, and enhancing prognosis monitoring.

Mammalian polo-like kinase 1 (PLK1), a member of the serine/threonine protein kinase family, exerts a crucial role during mitosis in mammals (Archambault and Glover 2009; Kalous and Aleshkina 2023). The ablation or inhibition of the PLK1 gene leads to abnormal chromosome segregation, resulting in mitotic arrest and often accompanied by cell death (Iliaki et al. 2021). Various studies have demonstrated that the expression of PLK1 is frequently elevated across a wide range of human malignancies and has been linked to unfavorable outcomes in patients with cancer (Fang et al. 2022; Zhao et al. 2023; Chen et al. 2024). Notably, blocking PLK1 expression *via* antibodies, small interfering RNA (siRNA), or kinase inhibitors effectively suppresses tumor development (Kumar and Kim 2015; Xu et al. 2023). Given its critical role in mitotic processes and its high expression levels in various cancers, PLK1 may represent an attractive target for cancer therapy (Elsayed et al. 2019). Despite the well-documented role of PLK1 in multiple cancers, its specific functions and mechanisms in BLCA remain largely underexplored. Further research into PLK1's molecular mechanisms in BLCA is essential to elucidate its potential as a therapeutic target and to develop more effective treatment strategies for this disease.

In various organisms, including mammals, the Hippo pathway plays a crucial role in controlling organ dimensions, facilitating tissue regeneration, and determining cellular fate (Patel et al. 2017; Fu et al. 2022). This pathway primarily functions by negatively regulating the transcriptional coactivators of Yes-associated protein (YAP), thereby inhibiting cell proliferation and promoting apoptosis (Liu et al. 2020; Cunningham and Hansen 2022). When the Hippo pathway is activated, a kinase cascade involving the mammalian STE20-like kinase 1 and 2 (MST1/2) and the large tumor suppressor kinase 1 and 2 (LATS1/2) phosphorylates YAP, inducing their cytoplasmic retention and subsequent degradation or inactivation (Kim and Jho 2018). Given that the loss of proteins encoded by the Hippo pathway can lead to cell proliferation, the disturbances within this pathway have been identified across numerous forms of human cancers (Maugeri-Saccà and De Maria 2016; Yeung et al. 2016; Pandurangan et al. 2018; Masliantsev et al. 2021). Alterations in the Hippo pathway have been implicated in promoting cell invasion, migration, disease progression, and therapeutic resistance in cancer (Mohajan et al. 2021). Therefore, understanding the specific mechanisms by which the Hippo pathway is dysregulated in BLCA is crucial for developing targeted therapies aimed at curbing tumor progression.

In this study, we discovered and evaluated potential biomarkers for diagnosing and treating BLCA using publicly available genetic datasets. Furthermore, we investigated the regulatory mechanisms of the key biomarker at both cellular and animal levels. Notably, PLK1 emerged as a significant focus of our research. By identifying common genes associated with PLK1 and BLCA, we explored potential pathways through which PLK1 might exert its effects on BLCA. This research aims to provide a theoretical foundation for developing new therapeutic strategies and drug targets for BLCA, ultimately contributing to improved patient outcomes and advancing our understanding of BLCA pathogenesis.

Materials and Methods

Differentially expressed genes (DEGs) selection

Our study involved an analysis of gene expression patterns obtained from the Gene Expression Omnibus (GEO) repository, a service provided by the National Center for Biotechnology Information (NCBI) in the United States (https://www.ncbi.nih.gov/geo/). Datasets related to "Bladder Cancer" were extracted and meticulously filtered, resulting in the selection of two appropriate datasets: GSE38264 and GSE130598. DEGs were identified utilizing the GEO2R tool (www.ncbi.nlm.nih.gov/geo/geo2r). DEGs between tumor and control samples were determined in both datasets based on stringent criteria of a p-value < 0.05 and a log fold change ($|\log FC| \geq 1$). Data normalization and batch effect correction were executed using the normalizeBetweenArrays function from the Limma package in R, with the results visually represented by box plots. DEGs were further elucidated using volcano plots and heat maps for visualization. Subsequently, a Venn diagram was utilized to depict the overlap of DEGs from the two datasets, emphasizing the common DEGs.

Functional enrichment analysis of common DEGs

The pathway analyses of Gene Ontology (GO) and Kyoto Encyclopedia of Genes and Genomes (KEGG) were carried out using the Database for Annotation, Visualization, and Integrated Discovery (DAVID; https://david.ncifcrf.

gov/summary.jsp). The outcomes from the GO enrichment analysis were organized into three primary categories: Molecular Function (MF), Biological Process (BP), and Cellular Component (CC). Subsequently, enrichment dot plots were created utilizing the R software package "ggplot2", with the minimum *p*-value selected to denote the most significant enrichment.

Protein-protein interaction (PPI) network and hub genes

To construct the PPI network and identify hub genes, we initially utilized the Search Tool for the Retrieval of Interaction Gene (STRING) database (https://www.string-db.org/) to establish a PPI network based on the common DEGs. The significance threshold for interaction confidence was set at a score of 0.400. After that, we employed Cytoscape software to visualize and analyze the PPI network. To detect molecular complexes within the PPI network, we used the "Molecular Complex Detection (MCODE)" plugin in Cytoscape. For further refinement of key genes, we applied the cytoHubba plugin for topological analysis within Cytoscape, based on the degree of centrality. We selected the top 10 hub genes with the highest degree centrality nodes as candidate hub genes.

Analysis of hub genes

The expression data of hub genes identified within the PPI network module were extracted from the expression profiles of GSE38264 and GSE130598, and the differential expression patterns were visualized using the "ggplot2" package in R. To elucidate the distribution of hub genes across different sample datasets, we employed the "ggridges" package in R to generate ridgeline plots utilizing the expression profile data from GSE38264 and GSE130598 datasets. Additionally, the relationships between proteins and pathways, along with variations in pathway functional strength, were depicted through GO enrichment chord diagrams created using the "GOplot" package in R. Principal component analysis (PCA) was conducted on the expression levels of hub genes across the GSE38264 and GSE130598datasets, utilizing the "prcomp" function in R. The expression levels of several hub genes were verified utilizing the Gene Expression Profiling Interactive Analysis (GEPIA) database (http://gepia.cancer-pku.cn/).

Receiver operating characteristic (ROC) curves

To assess the diagnostic performance of the selected hub genes, we utilized gene expression data from the two datasets and BLCA datasets in the Cancer Genome Atlas (TCGA) database (https://cancergenome.nih.gov/). Subsequently, the pROC package in R was employed to generate ROC curves for these hub genes. The area under the curve (AUC) was calculated for each ROC curve, providing a quantitative measure of the diagnostic performance. According to standard thresholds, an AUC value greater than 0.7 was considered to indicate a significant diagnostic value.

Downstream pathway identification

To identify downstream pathways associated with BLCA, we retrieved genes related to BLCA from the GeneCards database (https://www.genecards.org/Search). We then used the Coxpresdb database (https://coxpresdb.jp) to identify co-expressed genes of the target gene and performed a cross-analysis of these two sets of genes using a Venn diagram tool. The common genes were subjected to KEGG analysis using the bioinformatics database DAVID (https://david.ncifcrf.gov/summary.jsp). Pathways with a p-value < 0.05 were selected for further analysis, and an enrichment analysis bubble chart was generated to visualize these findings.

Cell culture and treatment

Human primary bladder epithelial cells were cultivated in specialized medium for primary epithelial cells, supplemented with 10% fetal bovine serum (FBS; Gibco, California, USA) and 1% antibiotic-antimycotic solution (Gibco). Similarly, human BLCA cell lines, T-24 and 5637 cells were maintained in MCCOY'S 5A (Thermo Fisher Scientific, Waltham, MA, USA) and RPMI-1640 (Thermo Fisher Scientific) media, respectively, each supplemented with 10% FBS and 1% antibiotic-antimycotic solution. All cell lines were sourced from iCell Bioscience Inc. (Shanghai, China). Cells were cultured at 37°C in a humidified incubator with 5% CO_2. The T-24 and 5637 cells were divided into the Control group: untreated cells; si-NC group: cells transfected with non-targeted siRNA (GeneChem, Shanghai, China); si-PLK1 group: cells transfected with siRNA targeting PLK1 (GeneChem); si-NC+MY-875 group: cells transfected with non-targeted siRNA and incubated with 0.92 μM MY-875 (Hippo pathway agonist; MedChemExpress, New Jersey, USA) for 48 h; si-PLK1+TDI-011536 group: cells transfected with siRNA targeting PLK1 and incubated with 3 μM TDI-011536 (Hippo pathway inhibitor; MedChemExpress) for 24 h.

To knock down the expression of PLK1 in BLCA cells, siRNAs targeting PLK1 (si-PLK1-1,-2,-3) were applied, with non-targeting siRNA serving as the control. The Lipo3000™ reagent kit (Thermo Fisher Scientific) was employed for the transfection of the cells according to the instructions. The sequence of siRNA was shown in Table S1 in Supplementary material. Transfection efficiency was evaluated by reverse transcription-quantitative polymerase chain reaction (RT-qPCR).

Cell counting Kit-8 (CCK-8) assay

To assess the effects of different treatments on the viability of T-24 and 5637 cells, a CCK-8 assay was employed. Initially, a 100 µl cell suspension (1×10^3 cells *per* well) was prepared in a 96-well plate and pre-incubated for 24 h at 37°C with 5% CO_2. The medium was then replaced with maintenance medium containing 200 µg/ml of the cell suspension, and the plate was returned to the incubator for further incubation periods of 24, 48, and 72 h. At each designated time point, the cells were rinsed twice with Dulbecco's phosphate-buffered saline (PBS), and each well was replenished with 90 µl of maintenance medium and 10 µl of CCK-8 solution, followed by an additional 2-h incubation. Absorbance was measured hourly to determine the optimal incubation time. Finally, the optical density value at 450 nm was measured using a microplate reader to determine the relative cell viability.

Transwell assay

To evaluate the invasion of T-24 or 5637 cells, a Transwell assay was conducted. Matrigel (MedChemExpress) was diluted at a ratio of 1:8 and used to coat the upper chamber of the Transwell inserts, which were then incubated at 37°C for 30 min. The basement membrane was then rehydrated before use. Cells were trypsinized, centrifuged to remove the culture medium, washed with PBS, and resuspended in serum-free medium containing bovine serum albumin. Cell suspension (100 µl) was added to each Transwell insert (1×10^5/well), and the lower chamber was filled with 600 µl of medium containing 20% FBS. After a 24-h incubation period under standard culture conditions, the inserts were removed, and the medium was discarded. The inserts were washed twice with calcium- and magnesium-free PBS, fixed with 4% paraformaldehyde for 30 min, and then stained with 0.1% crystal violet for 20 min, followed by gently wiping away of the non-migrated cells on the upper surface of the membrane. After washing three times with PBS, the inserts were examined under a microscope, photographed, and counted to assess the invasion of the cells.

Wound-healing assay

To assess the migratory capacity of T-24 or 5637 cells, a wound-healing assay was performed. Cells were seeded into 6-well plates at a density of 5×10^5 cells *per* well, and resuspended in 2 ml of complete culture medium and transferred to 6-well plates. The following day, once the cells had adhered and reached over 80% confluence, a scratch was made using a pipette tip held perpendicular to the underlying lines on the plate's back, ensuring that the tip remained vertical without tilting. The cells were rinsed three times with PBS to remove any detached cells, followed by adding a serum-free medium. The plates were then incubated at 37°C with 5% CO_2. Images were captured immediately (time point 0) and after 24 h of incubation. The migratory ability of the cells was analyzed using ImageJ software.

5-ethynyl-2'-deoxyuridine (EDU) assay

Cell proliferation was assessed with an EDU kit (Beyotime, Shenzhen, China). To label cells with EDU, they were incubated with an EDU working solution for 2 h. After EDU labeling, the culture medium was removed, and the cells were fixed with 1 ml of fixation solution for 15 min. Following this, the cells were permeabilized with 1 ml of permeabilization solution for 10 min, and 0.5 ml of Click Additive solution was added to each well. Samples were then incubated for 30 min in the dark. Afterward, the cells were washed three times with wash buffer for 5 min each. Next, cell nuclei were stained with 4',6-diamidino-2-phenylindole for 5 min. Finally, samples were observed and photographed under a fluorescence microscope.

Subcutaneous tumor experiment

To investigate the effect of PLK1 knockdown on tumor growth *in vivo*, a total of 12 male C57BL/6 mice (SPF Biotechnology Co., Ltd., Beijing, China), aged 6–8 weeks and weighing 18–20 g, were randomly divided into two groups: LV-si-NC group and LV-si-PLK1 group, with six mice *per* group. T-24 cells were transduced with lentivirus to knock down PLK1 expression. Subsequently, a subcutaneous xenograft tumor model was established by injecting transfected T-24 cells (2×10^6) into the right dorsal flank of each mouse. Tumor dimensions were measured every seven days using electronic Vernier calipers with the formula $V = ½ ab^2$ (where "a" was the maximum diameter of the tumor and "b" was the minimum diameter). On day 28 after post-injection, all mice were anesthetized with a 1.5% isoflurane-oxygen mixture for 5 min, followed by euthanasia through cervical dislocation to retrieve the xenografts. Tumor weight was measured over time, and tumor growth curves were plotted with tumor volume as the vertical axis and time as the horizontal axis.

All animal experiments were carried out with rigorous compliance to the ethical principles governing animal research, specifically adhering to the "Guide for the Care and Use of Laboratory Animals, 8th Edition" (Care and Animals 2011). The experimental protocols were approved by the Ethics Review Board of the Affiliated Hospital and Clinical Medical College of Chengdu University (Protocol Number: PJ2024-008-02), aligning closely with the ARRIVE guidelines version 2.0. The methods employed in animal care and experimentation were meticulously

reviewed and endorsed by our institution's Institutional Animal Care and Use Committee (IACUC). This ensured full compliance with both institutional and governmental regulations pertaining to the humane treatment of animals, thereby upholding the highest ethical standards throughout the research process.

Hematoxylin-Eosin (HE) staining

After harvesting the mouse xenograft tumor tissues, they were fixed in 4% paraformaldehyde solution for 24 h. The next day, the tissues were dehydrated through a graded ethanol gradient series of 50%, 70%, 80%, 90%, 95%, and absolute ethanol. After dehydration, the tissues were immersed in a 1:1 solution of absolute ethanol and xylene for 30 min, followed by immersion in pure xylene until they became transparent. Samples were embedded in paraffin wax. The tissue was positioned on a paraffin block base, and the block was trimmed to create a flat surface. The tissue was then sectioned into 4-μm-thick slices.

HE staining was employed to examine the alterations in mouse xenograft tumor tissues. The detailed procedure is as follows: The paraffin sections were baked at 60°C for 2 h, then deparaffinized using xylene and rehydrated through a graded alcohol series to water. The tissues were stained with hematoxylin for 10 min, rinsed under running water to remove excess stain, differentiated in 0.7% hydrochloric acid ethanol for 2 s, and rinsed again under running water until the sections turned blue. Sections were then dehydrated through 95% ethanol for 30 s, stained with eosin for 30 s, and dehydrated again. The sections were cleared in a 1: 4 mixture of lime carbonate and xylene for 30 s, followed by two changes of pure xylene, each for 30 s. Finally, the sections were mounted with neutral resin and examined under an optical microscope for staining results.

Immunohistochemical staining

Immunohistochemical staining was performed to detect the positive expression of Ki67 in tissues. The slides were subjected to antigen retrieval with citrate buffer for 25 min. After antigen retrieval, the sections were incubated with 0.3% hydrogen peroxide to inactivate the enzyme and washed with PBS, followed by blocking with 3% bovine serum albumin. Then, the sections were incubated overnight at 4°C with a rabbit anti-Ki67 primary antibody (Abcam, Cambridge, UK; ab15580; 1:400), followed by an 80-min incubation with a horseradish peroxidase-conjugated goat anti-rabbit IgG secondary antibody (Abcam; ab6721; 1:200). The sections were developed with diaminobenzidine and counterstained with hematoxylin. Finally, the slides were mounted with neutral resin and examined under a microscope.

RT-qPCR

To extract RNA from cells and tissues, TRIzol reagent (1 ml) was employed. RNA concentrations were determined using a Nano-100 spectrophotometer (Allsheng, Hangzhou, China). cDNA synthesis was performed utilizing the SweScript All-in-One First-Stand cDNA Synthesis Supermix for qPCR kit (Seville Biotechnology Co., Ltd., Wuhan, China). The reverse transcription reaction was conducted under the following conditions: 25°C for 5 min, 42°C for 30 min, and 85°C for 5 s. The synthesized cDNA was subsequently used for qPCR analysis. qPCR was performed on an ABI7500 PCR System (Applied Biosystems, Foster City, CA, USA) using the SYBR Premix Ex Taq II (#RR420A; Takara, Otsu, Shiga, Japan). The PCR protocol included: initial denaturation at 95°C for 30 s; a cycle of 40 repetitions, each including denaturation at 95°C for 10 s, annealing and extension at 60°C for 30 s, a final extension step at 60°C for 60 s; a hold step at 95°C for 15 s. Primers specific to the target genes were designed to evaluate mRNA expression levels, with GAPDH serving as an internal control. The relative expression levels were calculated using the $2^{-\Delta\Delta Ct}$ method. Primer sequences used in this study were detailed in Table S2.

Western blot

Proteins were extracted from cellular and tissue samples, resolved *via* 10% sodium dodecyl sulfate-polyacrylamide gel electrophoresis, and then transferred to polyvinylidene difluoride membranes. After transfer, the membrane was subjected to a blocking step with 5% non-fat dry milk for 2 h. Primary antibodies against PLK1 (Abcam, ab17057; dilution 1:2000), YAP (Abcam, ab205270; dilution 1:2000), and LATS1 (Abcam, ab70561; dilution 1:2000) were diluted in 5% non-fat dry milk blocking solution and incubated overnight at 4°C. The membranes were then washed with Tris-buffered saline containing Tween (TBST) buffer. Subsequently, the horseradish peroxidase-conjugated secondary antibodies (1:5000; Abcam), were diluted in TBST and incubated with membranes for 1 h. Subsequently, the membrane was placed on the incubation plate of the Tanon 5200 chemiluminescent imaging system (Shanghai, China), and visualized utilizing an enhanced chemiluminescence substrate. Images were captured during the exposure process. Protein expression levels were quantified using ImageJ software, with GAPDH serving as an internal control reference.

Statistical analysis

Statistical analyses were performed using GraphPad Prism software. Data are presented as mean ± standard deviation (SD). For comparisons between two groups, an unpaired *t*-test was conducted. For comparisons involving more than

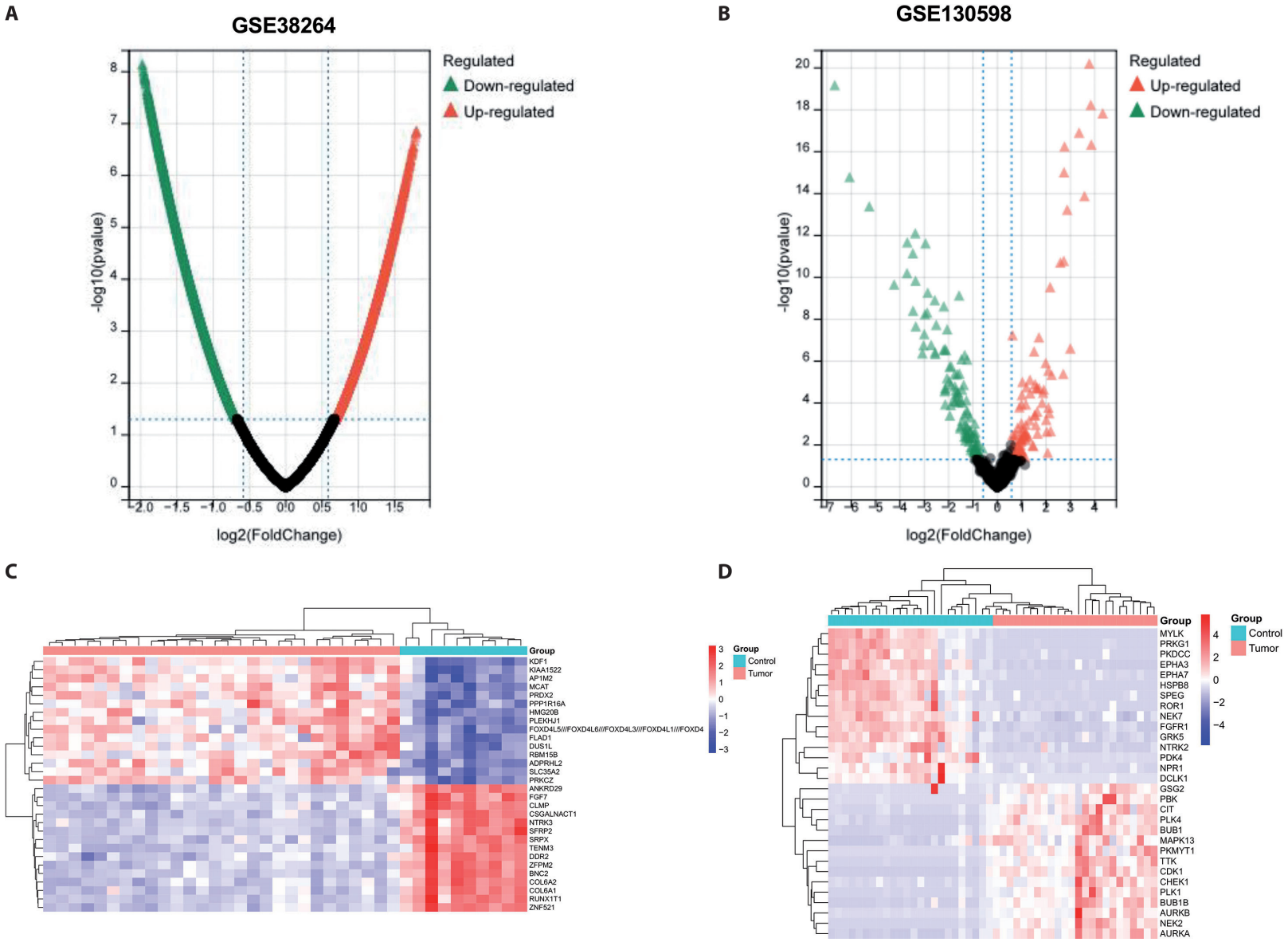

Figure 1. Selection of Differentially Expressed Genes (DEGs). Volcano plot of DEGs from the GSE38264 (**A**) and GSE130598 (**B**) dataset. Red dots represent up-regulated genes, blue dots down-regulated genes, and black dots represent genes that are not differentially expressed. Heat map of DEGs from the GSE38264 (**C**) and GSE130598 (**D**) dataset; the horizontal axis represents genes, with each column representing an individual sample. Red indicates high gene expression, and blue signifies low gene expression.

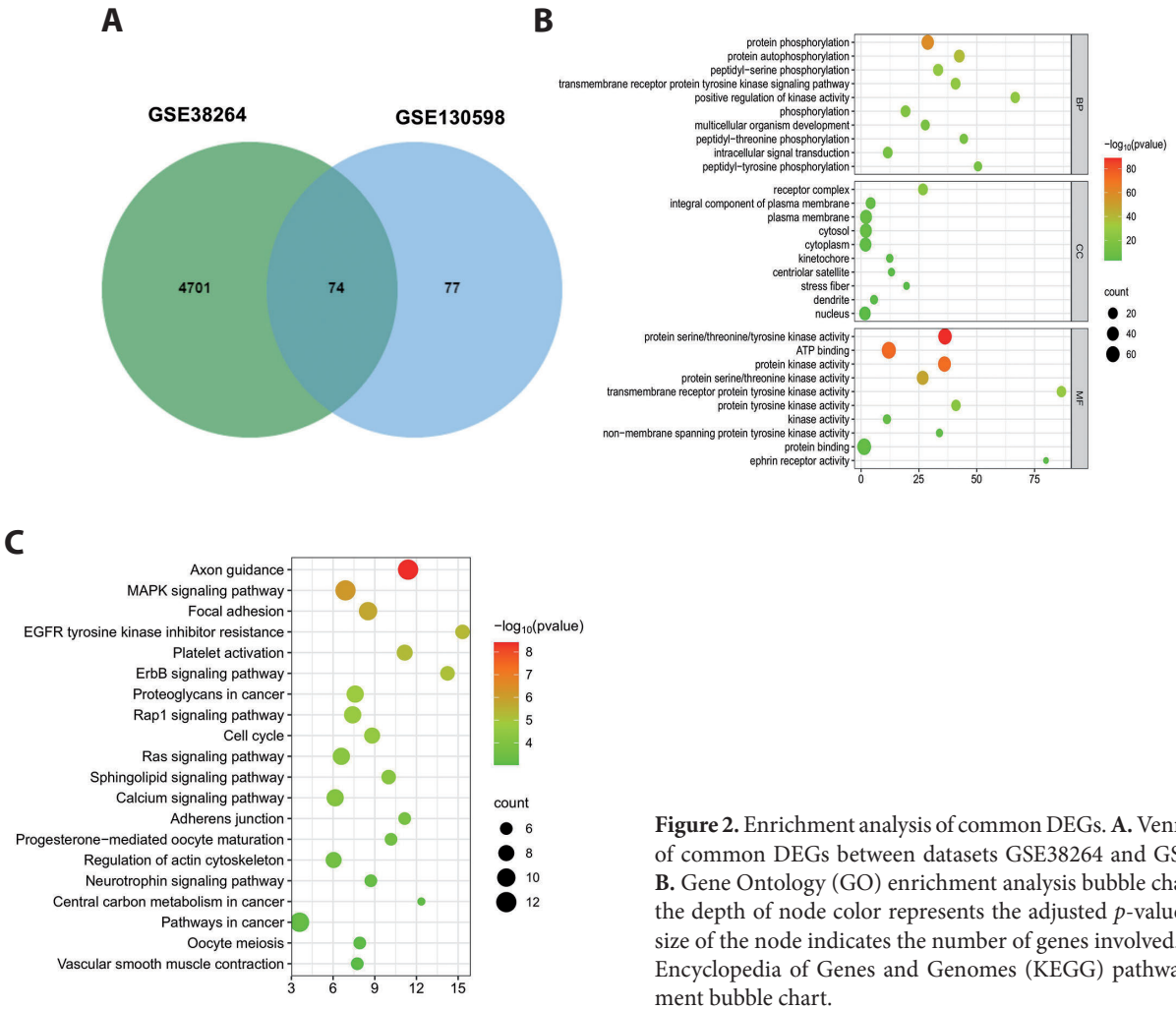

Figure 2. Enrichment analysis of common DEGs. **A.** Venn diagram of common DEGs between datasets GSE38264 and GSE130598. **B.** Gene Ontology (GO) enrichment analysis bubble chart, where the depth of node color represents the adjusted *p*-value, and the size of the node indicates the number of genes involved. **C.** Kyoto Encyclopedia of Genes and Genomes (KEGG) pathway enrichment bubble chart.

two groups, one-way ANOVA followed by Tukey's multiple comparisons test was applied to ascertain the significance of differences among groups.

Results

Identification of the BLCA-related DEGs

Data from the GSE38264 and GSE130598 datasets were normalized, and batch effects were corrected, demonstrating a significant reduction in batch-related variations and confirming effective batch effect control (Fig. S1). Using the GEO2R tool for differential expression analysis, we identified the significant DEGs from the GEO database. In the GSE38264 dataset, which included 10 normal bladder samples and 28 BLCA tissue samples, we selected DEGs based on a p-value ≤ 0.05 and |logFC| ≥ 1, yielding 4775 DEGs. Similarly, in the GSE130598 dataset, which included 24 normal adjacent tissue samples and 24 BLAC tissue samples, we identified 151 DEGs. Volcano plots of DEGs from the GSE38264 and GSE130598 datasets were generated to suggest differential expression and statistical significance (Fig. 1A,B). To further explore the expression patterns of these DEGs, we selected the top 15 upregulated and downregulated genes from each dataset and visualized using heat maps (Fig. 1C,D). The heat maps clearly illustrated differences in gene expression among samples and their clustering patterns. These visualizations indicated strong clustering effects and high confidence levels, further validating the accuracy and reliability of the identified DEGs. Additionally, we provide specific expression values for the top 15 upregulated and downregulated DEGs in both datasets (Table S3, S4).

Enrichment analysis of common DEGs

We intersected the DEGs from GSE38264 and GSE130598 datasets to identify common DEGs, and generated a Venn

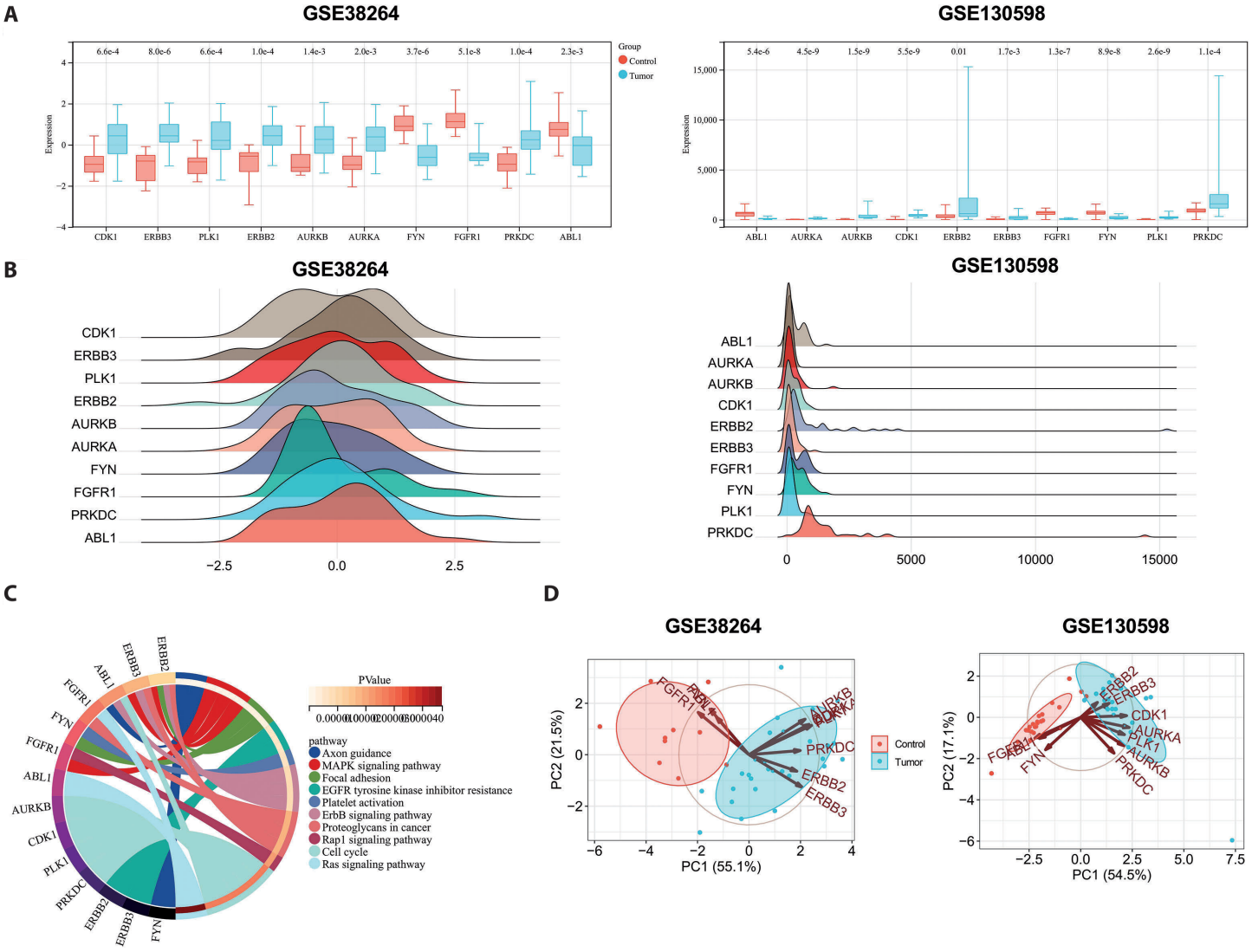

Figure 3. Key gene analysis. **A.** Boxplots representing gene expression levels across samples, with genes on the x-axis and expression values on the y-axis. **B.** Ridgeline plots displaying gene expression distributions, where the horizontal axis represents gene expression levels and the shape of the peaks indicates the dispersion among a group of data, with the height corresponding to the number of samples for each gene expression level. **C.** GO enrichment chord diagram comprising three sections: genes, LogFoldChange used for sorting and coloring gene blocks, and other columns representing GO terms, with different links indicating whether a gene belongs to a particular GO term. **D.** Principal component analysis of datasets GSE38264 and GSE130598, with PC1 and PC2 as the first and second principal components (indicating the variance explained by these latent variables), points representing samples, and different colors denoting distinct groups.

diagram to visualize the overlap (Fig. 2A). A total of 74 common DEGs were identified, we conducted GO and KEGG pathway enrichment analyses. We selected the top 10 most significantly enriched GO terms with the smallest *p*-values for each GO category and presented them in a GO enrichment bubble chart. The common DEGs were significantly enriched in BP terms such as "protein phosphorylation", "protein autophosphorylation", and "peptide-serine phosphorylation". In the CC category, the DEGs were notably enriched in terms of "receptor complex", "integral component of plasma membrane", and "plasma membrane". For MF, the DEGs were involved in "protein serine/threonine/tyrosine kinase activity", "ATP binding", and "protein kinase activity" (Fig. 2B). For the KEGG pathway analysis, we filtered the top 20 most significantly enriched pathways based on the smallest *p*-values and displayed these results in a KEGG pathway enrichment bubble chart. The KEGG results showed that the common DEGs were mainly enriched in pathways such as "Axon guidance", "MAPK signaling pathway", "Focal adhesion", "EGFR tyrosine kinase inhibitor resistance", and "Platelet activation" (Fig. 2C).

Hub gene selection

The PPI network was constructed and visualized using Cytoscape software (Fig. S2A). We identified statistically significant molecular complexes using the MCODE plugin (Fig. S2B). For further refinement of key genes, we applied the cytoHubba plugin for topological analysis within Cytoscape. The analysis identified the nodes with the highest degree of centrality as candidate hub genes, including ERBB2, ABL1, CDK1, AURKB, PLK1, FYN, AURKA, FGFR1, ERBB3, and PRKDC.

Analysis of hub genes

To further investigate the expression differences of ERBB2, ABL1, CDK1, AURKB, PLK1, FYN, AURKA, FGFR1, ERBB3, and PRKDC in the GSE38264 and GSE130598 datasets, we generated an expression difference plot, which illustrated the variation in gene expression levels across different samples (Fig. 3A). Additionally, ridgeline plots were constructed using the expression profile data from both datasets to visualize the distribution of these hub genes (Fig. 3B). A GO enrichment chord diagram was generated to depict the relationships between proteins and their associated pathways (Fig. 3C). Furthermore, we conducted a PCA analysis to evaluate the overall variability and distinguishing features of hub genes within the GSE38264 and GSE130598 datasets. This analysis yielded two principal components, PC1 and PC2, which accounted for 76.6% and 71.6% of the variance in the GSE38264 and GSE130598 datasets, respectively. These components proved effective separated control group samples from those in the BLCA group, as evidenced by the clear observed in the scatter plot using PC1 and PC2 as coordinates (Fig. 3D). These results further validated the reliability of PC1 and PC2 as robust indicators for classifying samples based on their genetic profiles.

Evaluation of the diagnostic value of hub genes in BLCA

To evaluate the diagnostic potential of the hub genes for BLCA, we plotted the ROC curves for these genes from both the GEO datasets and TCGA datasets. The results demonstrated that all hub genes had an AUC greater than 0.7 in both the GSE38264 and GSE130598 databases, indicating their strong diagnostic value for BLCA (Fig. S3, S4). In the TCGA database, AURKA, AURKB, CDK1, FGFR1, and PLK1 exhibited AUC values exceeding 0.9, while ABL1, ERBB2, ERBB3, FYN; and PRKDC demonstrated AUC values between 0.7 and 0.9, which further verified the robust predictive potential of hub gene (Fig. S5).

Validation of hub gene expression

We randomly measured the mRNA expression levels of several hub genes using RT-qPCR. The results indicated that, compared to the Control group, the mRNA expression levels of PLK1, AURKB, and CDK1 were significantly elevated in both T-24 and 5637 cells, whereas FYN expression was significantly reduced, which was consistent with the bioinformatics analysis (Fig. S6A). Furthermore, to corroborate these findings on a broader scale, we analyzed the data from the GEPIA database, which showed that compared to the Normal group, the Tumor group (BLCA) had significantly higher expression of PLK1, AURKB, and CDK1, while FYN expression was notably lower (Fig. S6B). This comprehensive approach robustly confirmed the differential expression patterns of these hub genes in BLCA, further validating the reliability of the bioinformatics analysis.

Knockdown of PLK1 inhibits the proliferation, migration, and invasion of BLCA cells

We conducted these hub genes through a PubMed literature search to confirm their novelty and relevance in current research. By integrating the results from MCODE, cytoHubba, and literature validation, PLK1 was ultimately identified as the target gene. PLK1 demonstrated significant centrality in all analyses and has not been widely reported in BLCA, aligning with our selection criteria.

To investigate the role of PLK1 in BLCA progression, we knocked down PLK1 expression in BLCA cell lines T-24 and 5637 (Fig. 4A). The results indicated that there was no

significant difference between the Control group and the si-NC group. However, PLK1 expression was significantly reduced in si-PLK1-11,-2, and -3 groups, with si-PLK1-1 showing the most effective knockdown. CCK-8 and EDU assays were used to assess the proliferation of BLCA cells in each group. The results demonstrated that compared to the si-NC group, the proliferation levels of BLCA cells in si-PLK1 groups were significantly decreased (Fig. 4B,C). Transwell assays were performed to evaluate cell invasiveness, revealing that the invasive capacity of BLCA cells in the si-PLK1 groups was significantly diminished compared to si-NC group (Fig. 4D). Additionally, wound-healing assays indicated a notable reduction in the migratory ability of BLCA cells in si-PLK1 groups relative to si-NC group (Fig. 4E).

Knockdown of PLK1 inhibits the occurrence and development of BLCA in mice

To verify the regulatory role of PLK1 in BLCA, we established a mouse xenograft tumor model by transfecting T-24 cells with lentivirus to knock down PLK1 expression. Western blot analysis showed that PLK1 expression was significantly reduced in the LV-si-PLK1 group compared to the LV-si-PLK1 group (Fig. 5A). Measurements of tumor weight and volume revealed a notable reduction in both parameters in

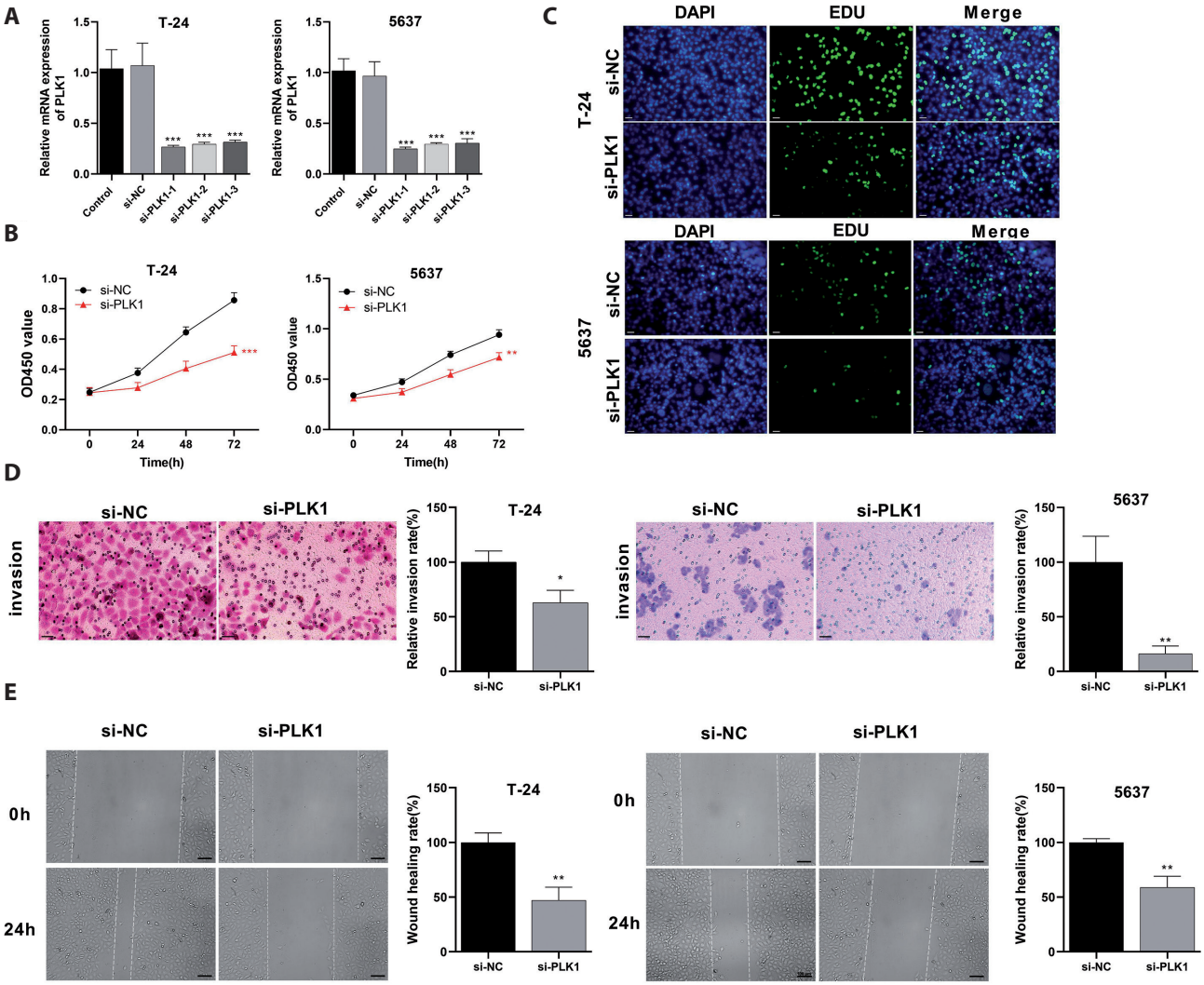

Figure 4. Knockdown of PLK1 inhibits the proliferation, migration, and invasion of bladder cancer cells. **A.** RT-qPCR analysis of the transfection efficiency of PLK1 in T-24 and 5637 cells. **B.** Cell Counting Kit-8 (CCK-8) assay measured the proliferation of T-24 and 5637 cells. **C.** Ethynyl-2-deoxyuridine (EDU) incorporation assay assessed the proliferation of T-24 and 5637 cells, scale: 100 μm. **D.** Transwell assay evaluated the invasive capabilities of T-24 and 5637 cells (magnification: 200×, scale: 100 μm). **E.** Wound-healing assay determined the migration of T-24 and 5637 cells (magnification: 100×, scale: 50 μm). * $p < 0.05$, ** $p < 0.01$, *** $p < 0.001$ *vs.* si-NC group.

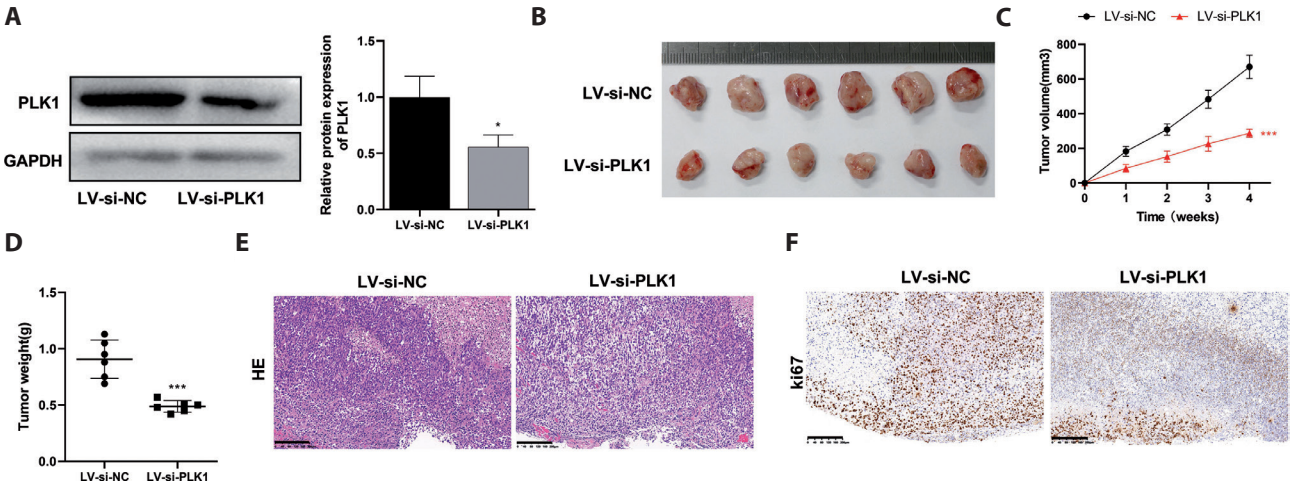

Figure 5. Knockdown of PLK1 inhibits the occurrence and development of bladder cancer in nude mice. **A.** Western blot analysis of PLK1 expression in tumor tissues from each group of nude mice. **B.** Representative images of xenograft tumors in nude mice. **C.** Growth curves of xenograft tumors in nude mice. **D.** Weight of xenograft tumors in nude mice. **E.** Hematoxylin and eosin (HE) staining of tumor tissue in each group (magnification: 100×, scale: 200 μm). **F.** Ki67 immunohistochemical staining assessed the proliferation levels of tumor cells (magnification: 100×, scale: 200 μm). $n = 6$; * $p < 0.05$, *** $p < 0.001$ *vs.* LV-si-NC group.

the LV-si-PLK1 group relative to the LV-si-NC group (Fig. 5B–D). HE staining was performed to assess cellular growth within the tumor tissues. Compared to the LV-si-NC group, tumors in the LV-si-PLK1 group exhibited considerable inflammatory cell infiltration, indicating a reduced malignancy level (Fig. 5E). Immunohistochemical staining was applied to detect the positive expression of Ki67 in tumor cells as an indicator of proliferation. The results demonstrated that the number of Ki67-positive cells in the LV-si-PLK1 group was markedly lower than in the LV-si-NC group (Fig. 5F).

Knockdown of PLK1 activates the Hippo pathway in BLCA

Using the Coxpresdb database, we identified 1,000 genes co-expressed with PLK1, which were then compared with 11,165 BLCA-related genes in a Venn diagram, yielding 572 overlapping genes (Fig. 6A). KEGG enrichment revealed that these common genes were primarily involved in the Hippo, RAP1, PI3K-Akt, and other signaling pathways (Fig. 6B). Among these, the Hippo pathway, which exhibited the most significant enrichment, was selected for further investigation. Western blot was used to detect the expression of Hippo pathway-related proteins, YAP and LATS1, in T-24 cells (Fig. 6C). The results showed that compared to the si-NC group, the expression of YAP was considerably reduced, while LATS1 expression was remarkably increased in both si-NC+MY-875 and si-PLK1 groups. Additionally, the expression of YAP in the si-PLK1+TDI-011536 group was significantly higher than in the si-PLK1 group, and LATS1 expression was significantly lower than in the si-PLK1 group. Consistent results were observed *in vivo*, with a significant reduction in YAP protein expression and a notable increase in LATS1 expression in tumor tissues of mice from the LV-si-PLK1 group compared to the LV-si-NC group (Fig. 6D).

Knockdown of PLK1 inhibits the proliferation, migration, and invasion of T-24 cells via activating the Hippo pathway

CCK-8 and EDU staining assays were employed to evaluate the proliferative activity of T24 cells. The results revealed that, in comparison to the si-NC group, both the si-NC+MY-875 and si-PLK1 groups exhibited a substantial decline in proliferative activity. Conversely, the si-PLK1+TDI-011536 group demonstrated a marked elevation in proliferation compared to the si-PLK1 group (Fig. 7A,B). Transwell and wound-healing assays were conducted to evaluate the invasive and migratory capacities of T24 cells. The findings revealed that both the si-NC+MY-875 and si-PLK1 groups displayed a significant suppression of invasion and migration compared to si-NC group. In contrast, the si-PLK1+TDI-011536 group exhibited a pronounced increase in invasion and migration capacities relative to the si-PLK1 group (Fig. 7C,D).

Discussion

Despite recent advancements in the management of BLCA, its inherent heterogenity and aggressive characteristics continue to pose challenges to accurate prognostic evaluation (Usuba et al. 2019). Herein, we identified PLK1, AURKA, AURKB, CDK1, ERBB2, ERBB3, FGFR1, FYN, ABL1, and

PRKDC as hub genes with predictive value for the diagnosis and treatment of BLCA. Among them, we verified that the expression levels of PLK1, AURKB, and CDK1 were upregulated in BLCA cell lines and tumor tissues, while FYN expression was downregulated. Mechanistically, the knockdown of PLK1 expression significantly impaired the viability, proliferation, migration, and invasion of BLCA cells. *In vivo*, PLK1 silencing suppressed tumor growth and development in nude mice. Furthermore, the Hippo pathway is a potential downstream pathway regulated by PLK1 in BLCA. Silencing PLK1 activated the Hippo pathway in BLCA. Notably, the inhibitor of the Hippo pathway reversed the suppressive effects of PLK1 silencing on the viability, proliferation, migration, and invasion of T-24 cells.

In this study, we corroborated the elevated expression of key genes – PLK1, AURKB, and CDK1 – in BLCA cells, as well as in publicly available clinical specimens from the TCGA database. Conversely, a significant reduction in FYN expression was consistently observed. By identifying BLCA-related DEGs in the GSE121711 and GSE130598 datasets and validating the central gene expression in 50 BLCA tumor samples and 50 adjacent normal bladder tissue samples, we found that PLK1 is significantly upregulated in tumor tissues, and patients with high PLK1 expression have a lower overall survival rate compared to those with low PLK1 expression (Liu et al. 2022). Bioinformatics analysis revealed that AURKB is highly expressed in patients with BLCA and is associated with prognosis, and its knockdown inhibits the proliferation, migration, invasion capabilities, and cell cycle progression of BLCA cells, thereby inducing cellular senescence (Li et al. 2024). Utilizing TCGA data to identify DEGs between BLCA tissues and adjacent normal tissues,

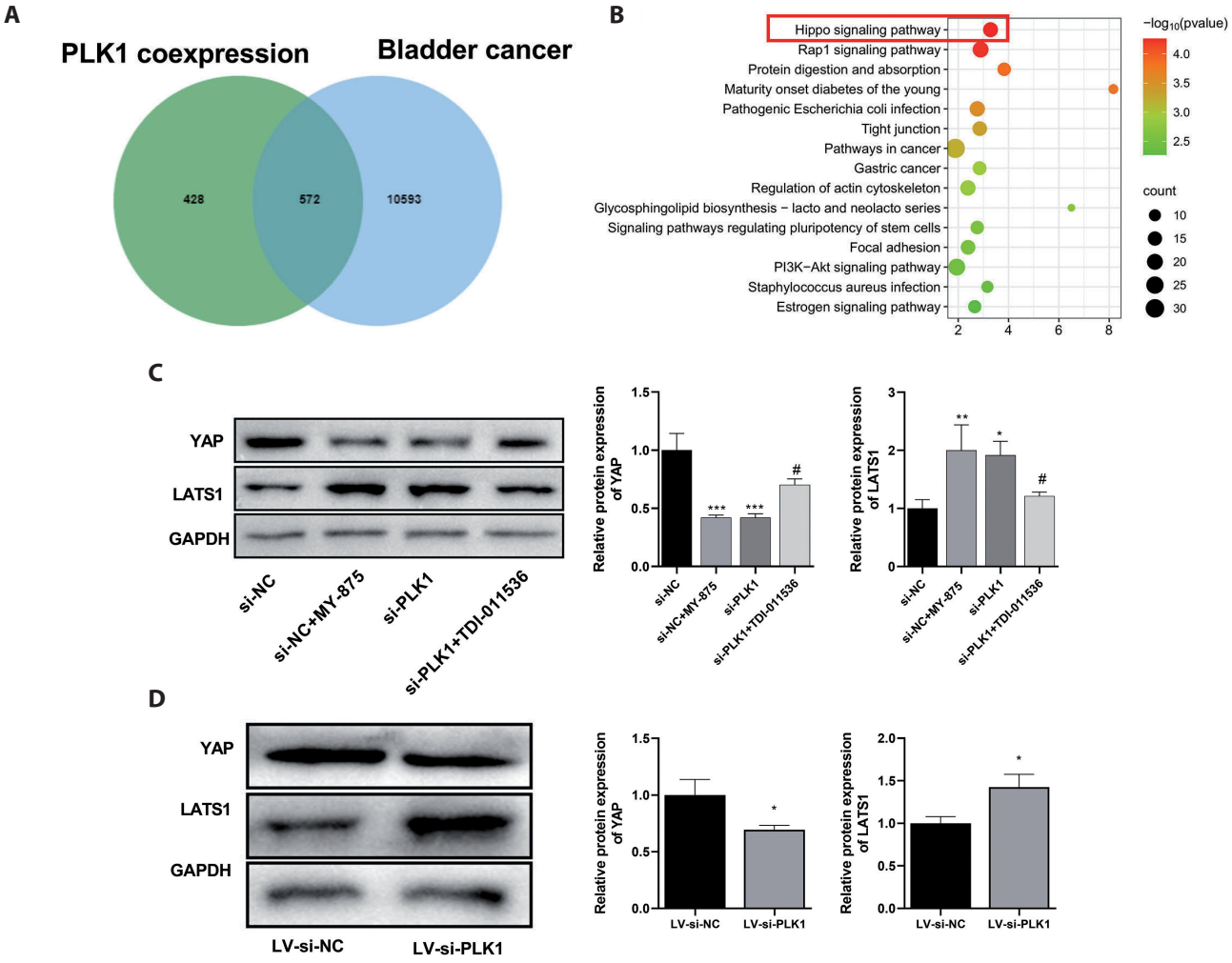

Figure 6. Downstream pathway screening. **A.** Venn diagram of the co-expressed genes of PLK1 and bladder cancer-related genes. **B.** KEGG enrichment analysis bubble chart for common genes. Western blot analysis of Hippo pathway-related protein expression *in vitro* (**C**) and *in vivo* (**D**). * $p < 0.05$, ** $p < 0.01$, *** $p < 0.001$ *vs.* si-NC group or LV-si-NC group; # $p < 0.05$ *vs.* si-PLK1 group or LV-si-PLK1 group.

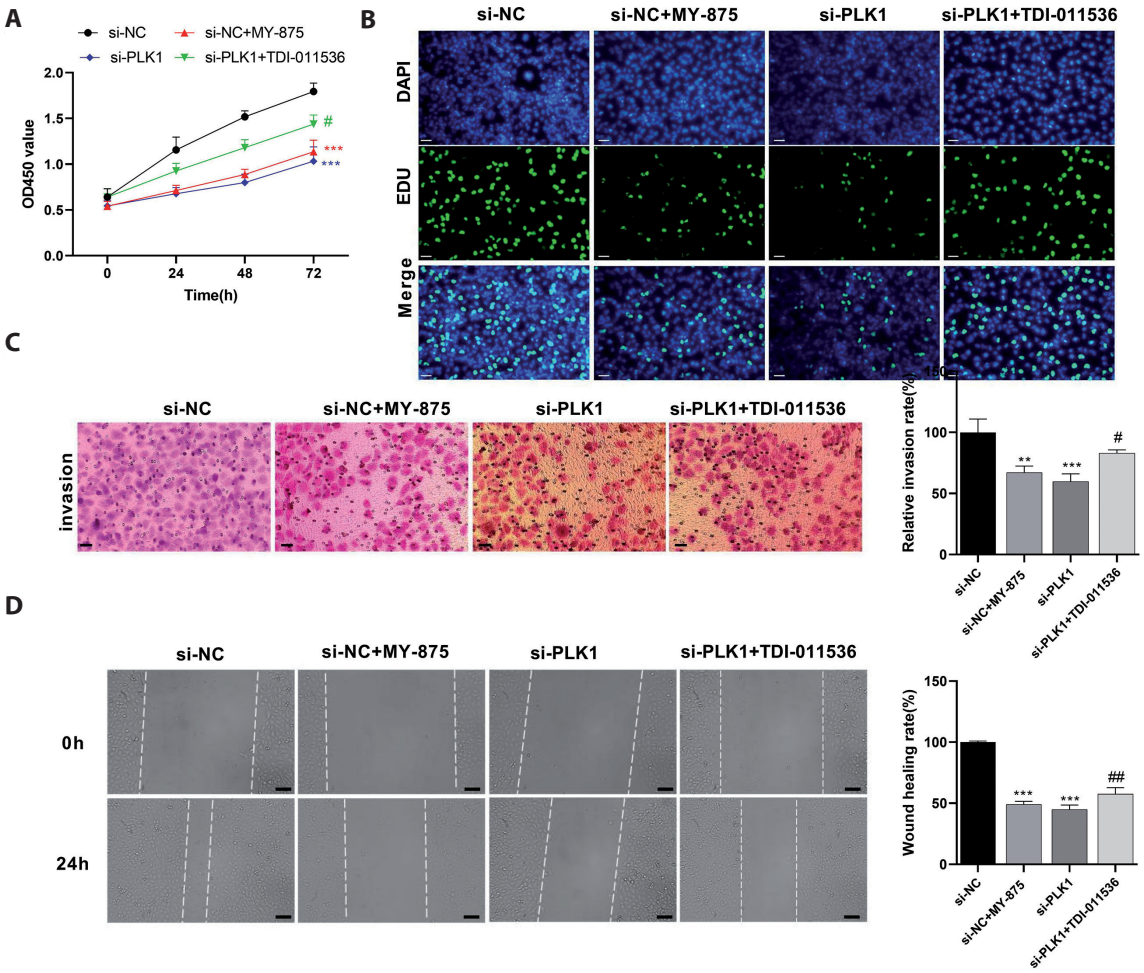

Figure 7. Knockdown of PLK1 inhibits the proliferation, migration, and invasion of T-24 cells *via* activating the Hippo pathway. **A.** CCK-8 assay measured the viability of cells in each group. **B.** EDU assay assessed cell proliferation in each group, scale: 100 μm. **C.** Transwell assay evaluated cell invasion (magnification: 200×, scale: 100 μm). **D.** Wound-healing assay determined cell migration (magnification: 100×, scale: 50 μm). ** $p < 0.01$, *** $p < 0.001$ *vs.* si-NC group; $^{\#}$ $p < 0.05$, $^{\#\#}$ $p < 0.01$ *vs.* si-PLK1 group.

followed by enrichment analysis and construction of a PPI network, revealed CDK1, PLK1, and AURKB as potential hub genes involved in various biological processes and signaling pathways, including apoptosis, Notch signaling, and Wnt/β-catenin signaling, all playing significant roles in BLCA (Danishuddin et al. 2024). Additionally, FYN, as a key hub gene in bladder urothelial carcinoma, is associated with the oncogenic role of cartilage oligomeric matrix protein in tumors (Guo et al. 2023). All in all, PLK1, AURKB, CDK1, and FYN are promising biomarkers with high predictive value in BLCA, holding significant implications for its prognosis and treatment.

PLK1 is widely recognized as an oncogene, playing a crucial role in numerous cell cycle-related activities (Meitinger et al. 2024). Research indicates that overexpression of PLK1 promotes carcinogenesis in prostate cancer, affecting cell reprogramming and promoting the migration and invasion of prostate cancer cells (Li et al. 2017). In a mouse xenograft model of metastatic castration-resistant prostate cancer resistant to abiraterone, the combination of a PLK1 inhibitor and abiraterone enhances mitotic arrest and significantly inhibits tumor cell growth (Patterson et al. 2023). In colorectal cancer, both genetic and pharmacological blockade of PLK1 significantly enhance sensitivity to oxaliplatin, while inhibiting the cell cycle mechanisms coupled with PLK1 can overcome the resistance of colorectal cancer to oxaliplatin (Yu et al. 2021). In the nude mouse model, the PLK1 inhibitor RO3280 impedes growth and obstructs the xenograft progression of BLCA (Zhang et al. 2017). Similar to the above results, we determined that silencing PLK1 significantly impaired the viability, proliferation, migration, and invasion of BLCA cells. *In vivo* studies showed that PLK1

knockdown hindered the growth and progression of BLCA tumors in nude mice. Taken together, these results highlight PLK1 as a promising therapeutic target for BLCA, with PLK1 knockdown suppressing tumor progression.

A series of studies have shown that the Hippo pathway is dysregulated in BLCA (Xia et al. 2018; Luo et al. 2021; Xie et al. 2023). The involvement of the Hippo pathway in BLCA progression may help identify new drug targets for BLCA management. In a study investigating the association between genetic variations in Hippo pathway genes and BLCA risk in the Chinese population, genetic variations in the WD repeat, coiled-coil containing 1 within the Hippo pathway have been found to reduce the risk of BLCA and may have a protective effect on the development of BLCA (Huang et al. 2020). Overexpression of miR-1307-5p can inhibit the growth of BLCA cells by suppressing the expression of the Mouse Double Minute 4 gene and its downstream Hippo pathway (Huang et al. 2022). Decitabine treatment can activate the Hippo pathway, thereby enhancing the cytotoxicity of cisplatin and doxorubicin against BLCA cells (Khandelwal et al. 2018). We found that knockdown of PLK1 activated the Hippo pathway in BLCA, showing effects similar to the Hippo pathway activator MY-875. Furthermore, the MY-875 treatment inhibited the viability, proliferation, migration, and invasion of BLCA cells. Further studies revealed that the Hippo pathway inhibitor reversed the suppressive effects of PLK1 silencing on the viability, proliferation, migration, and invasion of BLCA cells. In short, the knockdown of PLK1 inhibited BLCA *via* activating the Hippo pathway.

Our study has several limitations. For instance, the number of repetitions for experiments on cell lines was restricted to three due to constraints in experimental time and funding. To address this limitation, we implemented rigorous experimental protocols and meticulous data recording at every stage of the experiment. Additionally, we conducted thorough quality control checks to minimize any potential sources of error or bias. Furthermore, we performed *in vivo* animal experiments to further validate the role of PLK1 in BLCA cell lines from our *in vitro* studies.

In conclusion, our study identified and validated PLK1, AURKB, CDK1, and FYN as novel biomarkers with significant predictive value for the diagnosis and treatment of BLCA. The knockdown of PLK1 inhibits the development of BLCA by activating the Hippo pathway. These findings suggest that PLK1 plays a crucial role in BLCA progression, making it a promising therapeutic target. By targeting PLK1 and modulating the Hippo pathway, we can potentially develop novel and effective treatment strategies for BLCA management. This research holds significant clinical implications, offering new avenues for improving patient outcomes and enhancing precision medicine approaches in the fight against BLCA.

Ethics approval and consent to participate. The animal experiments were approved by the Affiliated Hospital and Clinical Medical College of Chengdu University ethical committee (PJ2024-008-02) in accordance with the ARRIVE guidelines 2.0. All methods related to animal care and use were approved by the Institutional Animal Care and Use Committee of our institute and strictly followed institutional and governmental guidelines for the ethical treatment of animals.

Availability of data and materials. The data that support the findings of this study are openly available in Gene Expression Omnibus at https://www.ncbi.nlm.nih.gov/geo/, reference number GSE38264 and GSE130598.

Conflict of interest. The authors declare that they have no conflict of interest.

Funding. This work is supported by Research on the Mechanism of CISD1 Gene Regulating Ferroptosis through Iron Homeostasis in the Proliferation of Bladder Cancer (Y202224) to Yue Yang, and Research on the Mechanism of METTL14-Mediated m6A Modification in Regulating the Proliferation and Metastasis of Clear Cell Renal Cell Carcinoma (Y202326) to Haifeng Hu.

Author contributions. Conceptualization: YY, ZZ; Methodology: YY, ZZ; Investigation: HCZ, YHW; Formal analysis: HCZ, YHW; Writing – Original draft: YY, ZZ; Writing – Review, Editing: YY, HCZ, HFH. All authors took part in the experiment. All authors read and approved the final manuscript.

Reference

Archambault V, Glover DM (2009): Polo-like kinases: conservation and divergence in their functions and regulation. Nat. Rev. Mol. Cell Biol. **10,** 265-275
https://doi.org/10.1038/nrm2653

Chen M, Zhang S, Wang F, He J, Jiang W, Zhang L (2024): DLGAP5 promotes lung adenocarcinoma growth via upregulating PLK1 and serves as a therapeutic target. J. Transl. Med. **22,** 209
https://doi.org/10.1186/s12967-024-04910-8

Compérat E, Amin MB, Cathomas R, Choudhury A, De Santis M, Kamat A, Stenzl A, Thoeny HC, Witjes JA (2022): Current best practice for bladder cancer: a narrative review of diagnostics and treatments. Lancet **400,** 1712-1721
https://doi.org/10.1016/S0140-6736(22)01188-6

Cunningham R, Hansen CG (2022): The Hippo pathway in cancer: YAP/TAZ and TEAD as therapeutic targets in cancer. Clin. Sci. **136,** 197-222
https://doi.org/10.1042/CS20201474

Danishuddin, Haque MA, Khan S, Kim JJ, Ahmad K (2024): Molecular landscape of bladder cancer: Key genes, transcription factors, and drug interactions. Int. J. Mol. Sci. **25,** 10997
https://doi.org/10.3390/ijms252010997

Dyrskjøt L, Hansel DE, Efstathiou JA, Knowles MA, Galsky MD, Teoh J, Theodorescu D (2023): Bladder cancer. Nat. Rev. Dis. Primers **9,** 58
https://doi.org/10.1038/s41572-023-00468-9

Elsayed I, Wang X (2019): PLK1 inhibition in cancer therapy: potentials and challenges. Future Med. Chem. **11,** 1383-1386 https://doi.org/10.4155/fmc-2019-0084

Facchini G, Cavaliere C, Romis L, Mordente S, Facchini S, Iovane G, Capasso M, D'Errico D, Liguori C, Formato R, et al. (2020): Advanced/metastatic bladder cancer: current status and future directions. Eur. Rev. Med. Pharmacol. Sci. **24,** 11536-11552

Fang L, Liu Q, Cui H, Zheng Y, Wu C (2022): Bioinformatics analysis highlight differentially expressed CCNB1 and PLK1 genes as potential anti-breast cancer drug targets and prognostic markers. Genes (Basel) **13,** 654 https://doi.org/10.3390/genes13040654

Flaig TW, Spiess PE, Abern M, Agarwal N, Bangs R, Boorjian SA, Buyyounouski MK, Chan K, Chang S, Friedlander T, et al. (2022): NCCN guidelines insights: Bladder cancer, Version 2.2022. J. Natl. Compr. Canc. Netw. **20,** 866-878 https://doi.org/10.6004/jnccn.2022.0041

Fu M, Hu Y, Lan T, Guan KL, Luo T, Luo M (2022): The Hippo signalling pathway and its implications in human health and diseases. Signal. Transduct. Target Ther. **7,** 376 https://doi.org/10.1038/s41392-022-01191-9

Guide for the Care and Use of Laboratory Animals. (2011), Eighth Edition, The National Academies Press, Washington, D.C.

Guo B, Wang Y, Liu W, Zhang S (2023): Cartilage oligomeric matrix protein acts as a molecular biomarker in multiple cancer types. Clin Transl Oncol. **25,** 535-554 https://doi.org/10.1007/s12094-022-02968-8

Huang W, Zhang C, Xiong S, Zhou X, Wang G, Guo J (2022): miR-1307-5p suppresses proliferation and tumorigenesis of bladder cancer via targeting MDM4 and the Hippo signaling pathway. Discov. Oncol. **13,** 57 https://doi.org/10.1007/s12672-022-00512-2

Huang Z, Wang X, Ma L, Guo Z, Liu H, Du M, Chu H, Wang M, Wang Z, Zhang Z (2020): Genetic variations in Hippo pathway genes influence bladder cancer risk in a Chinese population. Arch. Toxicol. **94,** 785-794 https://doi.org/10.1007/s00204-020-02663-z

Iliaki S, Beyaert R, Afonina IS (2021): Polo-like kinase 1 (PLK1) signaling in cancer and beyond. Biochem. Pharmacol. **193,** 114747 https://doi.org/10.1016/j.bcp.2021.114747

Jubber I, Ong S, Bukavina L, Black PC, Compérat E, Kamat AM, Kiemeney L, Lawrentschuk N, Lerner SP, Meeks JJ, et al. (2023): Epidemiology of bladder cancer in 2023: A systematic review of risk factors. Eur. Urol. **84,** 176-190 https://doi.org/10.1016/j.eururo.2023.03.029

Kalous J, Aleshkina D (2023): Multiple roles of PLK1 in mitosis and meiosis. Cells **12,** 187 https://doi.org/10.3390/cells12010187

Khandelwal M, Anand V, Appunni S, Seth A, Singh P, Mathur S, Sharma A (2018): Decitabine augments cytotoxicity of cisplatin and doxorubicin to bladder cancer cells by activating hippo pathway through RASSF1A. Mol. Cell. Biochem. **446,** 105-114 https://doi.org/10.1007/s11010-018-3278-z

Kim W, Jho EH (2018): The history and regulatory mechanism of the Hippo pathway. BMB Rep. **51,** 106-118 https://doi.org/10.5483/BMBRep.2018.51.3.022

Kumar S, Kim J (2015): PLK-1 targeted inhibitors and their potential against tumorigenesis. Biomed. Res. Int. **2015,** 705745 https://doi.org/10.1155/2015/705745

Li J, Wang R, Kong Y, Broman MM, Carlock C, Chen L, Li Z, Farah E, Ratliff TL, Liu X (2017): Targeting Plk1 to enhance efficacy of olaparib in castration-resistant prostate cancer. Mol. Cancer Ther. **16,** 469-479 https://doi.org/10.1158/1535-7163.MCT-16-0361

Li L, Jiang P, Hu W, Zou F, Li M, Rao T, Ruan Y, Yu W, Ning J, Cheng F (2024): AURKB promotes bladder cancer progression by deregulating the p53 DNA damage response pathway via MAD2L2. J. Transl. Med. **22,** 295 https://doi.org/10.1186/s12967-024-05099-6

Liu B, Meng LB, Su JZ, Fan B, Zhao SB, Wang HY, Li T, Wang TY, Zhang AL, Ni XC (2022): PLK1 as one novel target for the poor prognosis of bladder cancer: An observational study. Medicine **101,** e30723 https://doi.org/10.1097/MD.0000000000030723

Liu C, Wu Y, Ma J (2020): Interaction of non-coding RNAs and Hippo signaling: Implications for tumorigenesis. Cancer Lett. **493,** 207-216 https://doi.org/10.1016/j.canlet.2020.08.012

Lobo N, Hensley PJ, Bree KK, Nogueras-Gonzalez GM, Navai N, Dinney CP, Sylvester RJ, Kamat AM (2022): Updated European Association of Urology (EAU) prognostic factor risk groups overestimate the risk of progression in patients with non-muscle-invasive bladder cancer treated with bacillus calmette-guérin. Eur. Urol. Oncol. **5,** 84-91 https://doi.org/10.1016/j.euo.2021.11.006

Luo Y, Zhou J, Tang J, Zhou F, He Z, Liu T, Liu T (2021): MINDY1 promotes bladder cancer progression by stabilizing YAP. Cancer Cell. Int. **21,** 395 https://doi.org/10.1186/s12935-021-02095-4

Masliantsev K, Karayan-Tapon L, Guichet PO (2021): Hippo signaling pathway in Gliomas. Cells **10,** 184 https://doi.org/10.3390/cells10010184

Maugeri-Saccà M, De Maria R (2016): Hippo pathway and breast cancer stem cells. Crit. Rev. Oncol. Hematol. **99,** 115-122 https://doi.org/10.1016/j.critrevonc.2015.12.004

Meitinger F, Belal H, Davis RL, Martinez MB, Shiau AK, Oegema K, Desai A (2024): Control of cell proliferation by memories of mitosis. Science **383,** 1441-1448 https://doi.org/10.1126/science.add9528

Mohajan S, Jaiswal PK, Vatanmakarian M, Yousefi H, Sankaralingam S, Alahari SK, Koul S, Koul HK (2021): Hippo pathway: Regulation, deregulation and potential therapeutic targets in cancer. Cancer Lett. **507,** 112-123 https://doi.org/10.1016/j.canlet.2021.03.006

Pandurangan AK, Divya T, Kumar K, Dineshbabu V, Velavan B, Sudhandiran G (2018): Colorectal carcinogenesis: Insights into the cell death and signal transduction pathways: A review. World J. Gastrointest. Oncol. **10,** 244-259 https://doi.org/10.4251/wjgo.v10.i9.244

Patel SH, Camargo FD, Yimlamai D (2017): Hippo signaling in the liver regulates organ size, cell fate, and carcinogenesis. Gastroenterology **152,** 533-545 https://doi.org/10.1053/j.gastro.2016.10.047

Patterson JC, Varkaris A, Croucher PJP, Ridinger M, Dalrymple S, Nouri M, Xie F, Varmeh S, Jonas O, Whitman MA, et al.

(2023): Plk1 inhibitors and abiraterone synergistically disrupt mitosis and kill cancer cells of disparate origin independently of androgen receptor signaling. Cancer Res. **83,** 219-238 https://doi.org/10.1158/0008-5472.CAN-22-1533

Sanli O, Dobruch J, Knowles MA, Burger M, Alemozaffar M, Nielsen ME, Lotan Y (2017): Bladder cancer. Nat. Rev. Dis. Primers. **3,** 17022 https://doi.org/10.1038/nrdp.2017.22

Tran L, Xiao JF, Agarwal N, Duex JE, Theodorescu D (2021): Advances in bladder cancer biology and therapy. Nat. Rev. Cancer **21,** 104-121 https://doi.org/10.1038/s41568-020-00313-1

Usuba W, Urabe F, Yamamoto Y, Matsuzaki J, Sasaki H, Ichikawa M, Takizawa S, Aoki Y, Niida S, Kato K, et al. (2019): Circulating miRNA panels for specific and early detection in bladder cancer. Cancer Sci. **110,** 408-419 https://doi.org/10.1111/cas.13856

Witjes JA, Bruins HM, Cathomas R, Compérat EM, Cowan NC, Gakis G, Hernández V, Linares Espinós E, Lorch A, et al. (2021): European Association of Urology guidelines on muscle-invasive and metastatic bladder cancer: Summary of the 2020 guidelines. Eur. Urol. **79,** 82-104 https://doi.org/10.1016/j.eururo.2020.03.055

Xia J, Zeng M, Zhu H, Chen X, Weng Z, Li S (2018): Emerging role of Hippo signalling pathway in bladder cancer. J. Cell. Mol. Med. **22,** 4-15 https://doi.org/10.1111/jcmm.13293

Xie B, Lin J, Chen X, Zhou X, Zhang Y, Fan M, Xiang J, He N, Hu Z, Wang F (2023): CircXRN2 suppresses tumor progression driven by histone lactylation through activating the Hippo pathway in human bladder cancer. Mol. Cancer **22,** 151 https://doi.org/10.1186/s12943-023-01856-1

Xu R, Lee YJ, Kim CH, Min GH, Kim YB, Park JW, Kim DH, Kim JH, Yim H (2023): Invasive FoxM1 phosphorylated by PLK1 induces the polarization of tumor-associated macrophages to promote immune escape and metastasis, amplified by IFITM1. J. Exp. Clin. Cancer Res. **42,** 302 https://doi.org/10.1186/s13046-023-02872-1

Yeung B, Yu J, Yang X (2016): Roles of the Hippo pathway in lung development and tumorigenesis. Int. J. Cancer **138,** 533-539 https://doi.org/10.1002/ijc.29457

Yu Z, Deng P, Chen Y, Liu S, Chen J, Yang Z, Chen J, Fan X, Wang P, Cai Z, et al. (2021): Inhibition of the PLK1-coupled cell cycle machinery overcomes resistance to oxaliplatin in colorectal cancer. Adv. Sci. **8,** e2100759 https://doi.org/10.1002/advs.202100759

Zhang Z, Zhang G, Kong C (2017): Targeted inhibition of Polo-like kinase 1 by a novel small-molecule inhibitor induces mitotic catastrophe and apoptosis in human bladder cancer cells. J. Cell. Mol. Med. **21,** 758-767 https://doi.org/10.1111/jcmm.13018

Zhao M, Lu T, Bi G, Hu Z, Liang J, Bian Y, Feng M, Zhan C (2023): PLK1 regulating chemoradiotherapy sensitivity of esophageal squamous cell carcinoma through pentose phosphate pathway/ferroptosis. https://doi.org/10.1016/j.biopha.2023.115711

Received: December 10, 2024
Final version accepted: February 24, 2025

doi: 10.4149/gpb_2025015

Supplementary Material

Knockdown of PLK1 suppresses malignant phenotypes and tumor growth in bladder cancer *via* activating Hippo pathway

Yue Yang[1,*], Yunhan Wang[1,*], Zhou Zheng[2], Hanchao Zhang[1] and Haifeng Hu[1]

[1] *Department of Urology, The Affiliated Hospital and Clinical Medical College of Chengdu University, China*
[2] *Department of Urology, The Traditional Chinese Medicine Hospital of Longquanyi, Chengdu, China*

Supplementary Figures

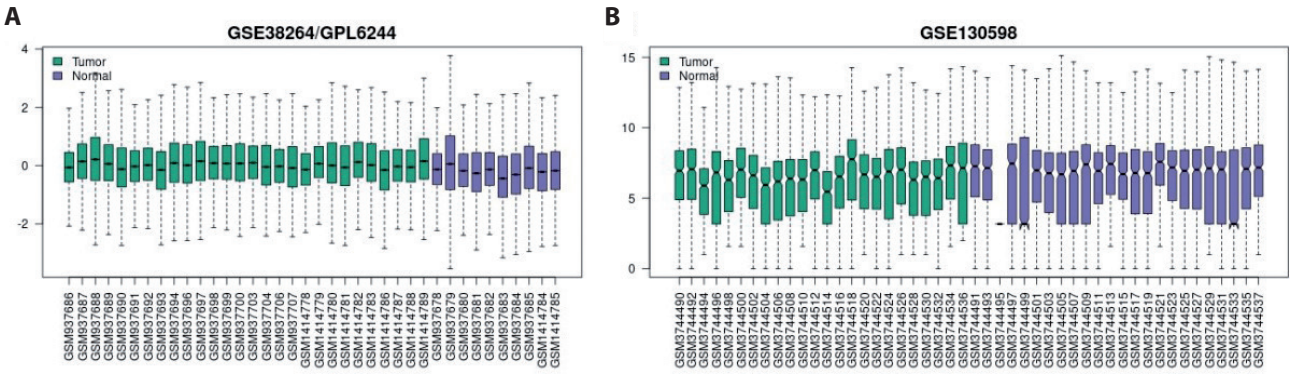

Figure S1. The box plot shows the result after data correction. **A.** Box plot of GSE38264 expression. **B.** Box plot of GSE130598 expression.

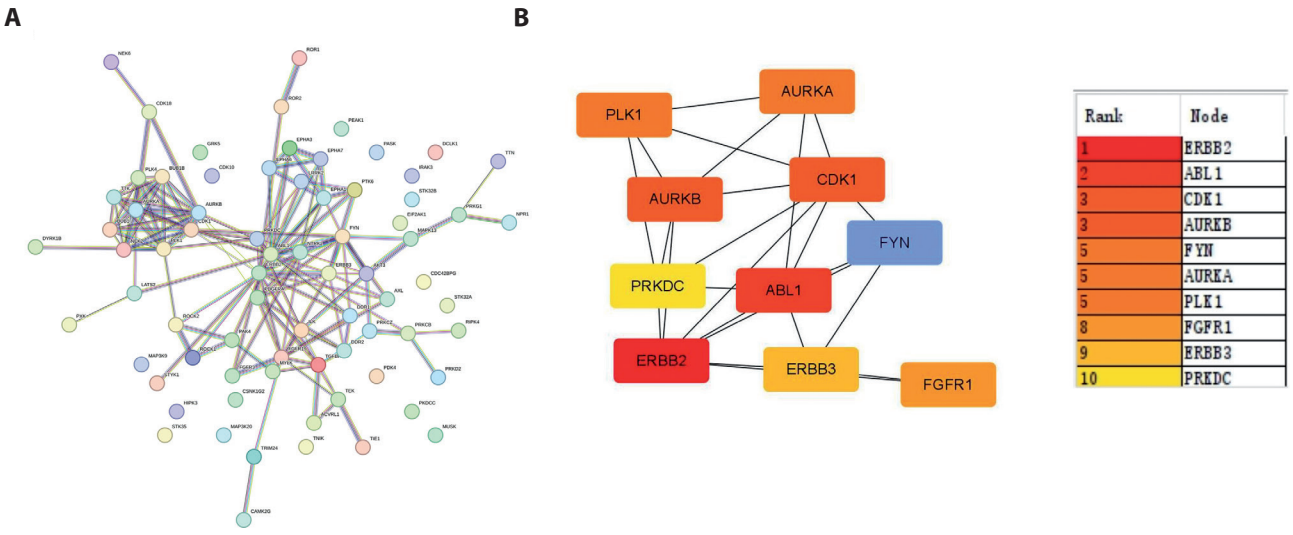

Figure S2. Hub gene identification. **A.** Protein-Protein Interaction (PPI) network. The lines between nodes represent interactions between genes. **B.** Key module containing the top 10 hub genes.

* These authors contributed equally to this work.

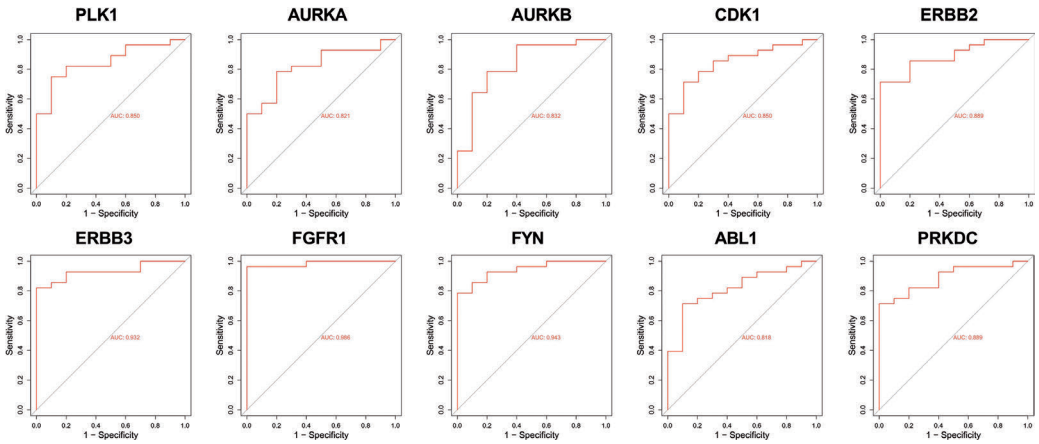

Figure S3. The Receiver Operating Characteristic (ROC) curves of hub genes in GSE38264. ROC curves for PLK1, AURKA, AURKB, CDK1, ERBB2, ERBB3, FGFR1, FYN, ABL1, and PRKDC.

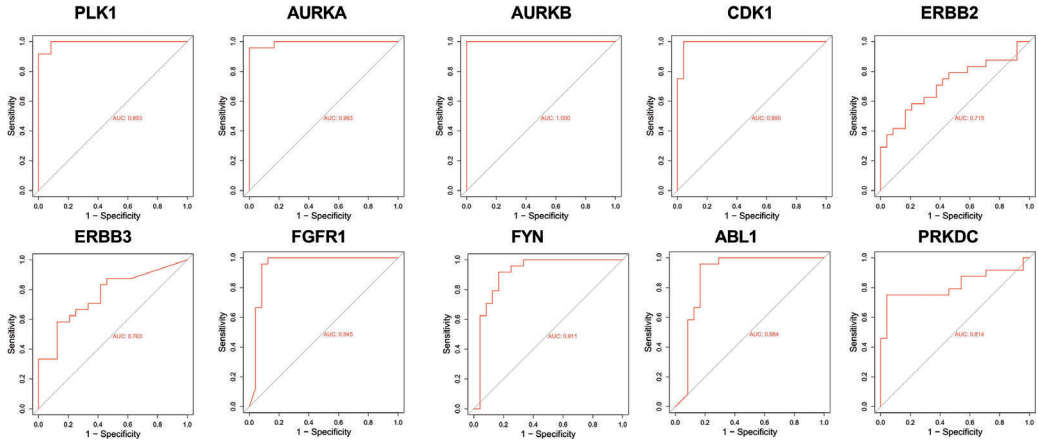

Figure S4. The ROC curves of hub genes in GSE130598: ROC curves for PLK1, AURKA, AURKB, CDK1, ERBB2, ERBB3, FGFR1, FYN, ABL1, and PRKDC.

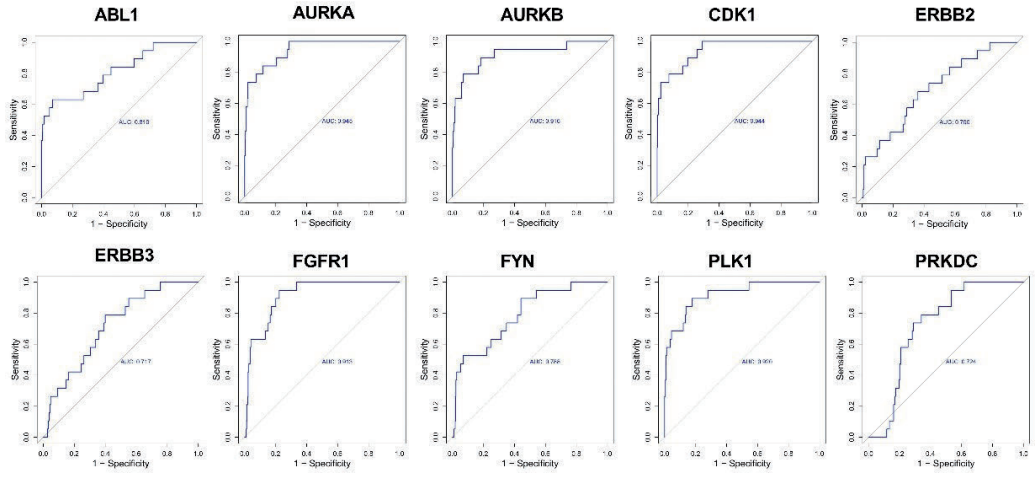

Figure S5. The ROC curves of hub genes in BLCA datasets of the Cancer Genome Atlas database: ROC curves for PLK1, AURKA, AURKB, CDK1, ERBB2, ERBB3, FGFR1, FYN, ABL1, and PRKDC.

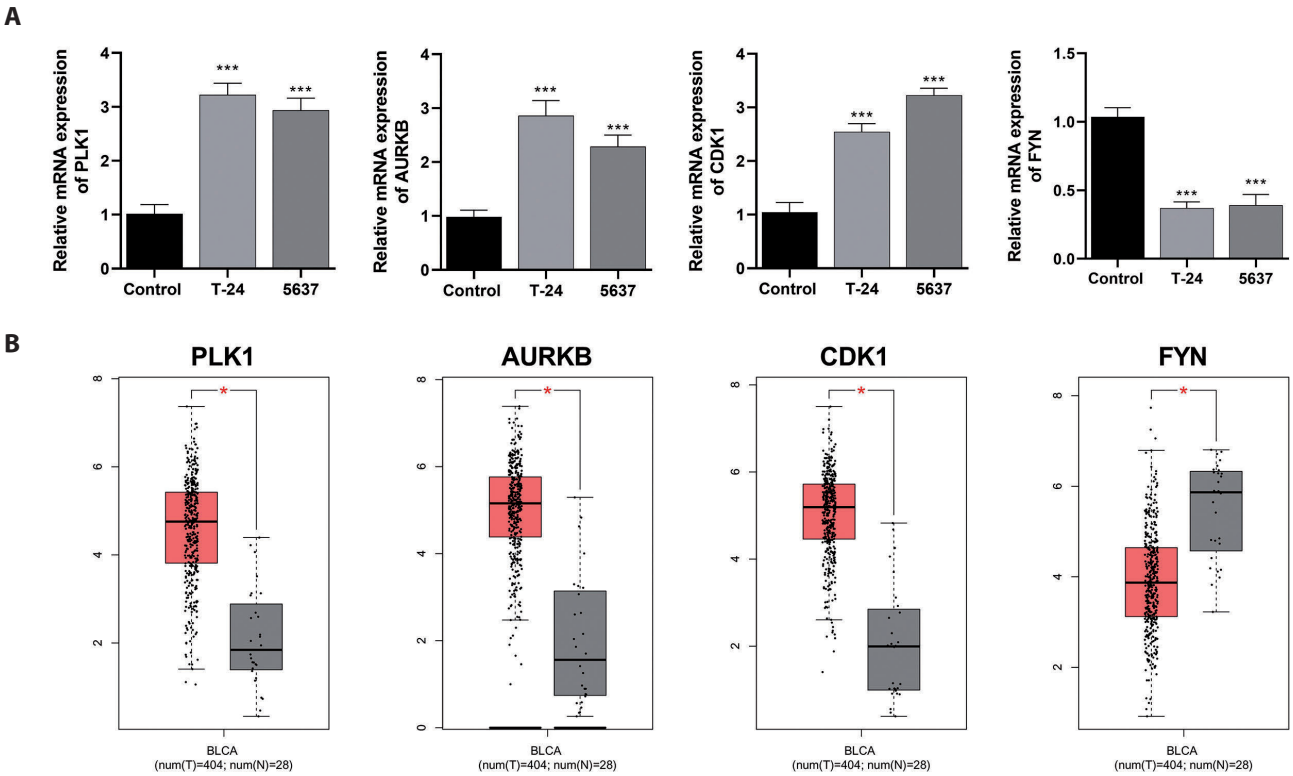

Figure S6. Validation of hub gene expression. **A.** RT-qPCR validation of mRNA expression levels for PLK1, AURKB, CDK1, and FYN. **B.** Expression of PLK1, AURKB, CDK1, and FYN in normal bladder tissue and bladder cancer tissue in the Gene Expression Profiling Interactive Analysis database. $n = 3$, * $p < 0.05$, *** $p < 0.001$ *vs.* Control group.

Supplementary Tables

Table S1. siRNA sequence

Name	Sequence (5'–3')
si-NC-F	UAUUUCCAUGGACAUCUUCUC
si-NC-R	GAAGAUGUCCAUGGAAAUAUC
si-PLK1-F-1	AUCUUCAUUCAGGAAAAGGUU
si-PLK1-R-1	CCUUUUCCUGAAUGAAGAUCU
si-PLK1-F-2	UCAUAUUCGACUUUGGUUGCC
si-PLK1-R-2	CAACCAAAGUCGAAUAUGACG
si-PLK1-F-3	ACUGUAUUCAUUCUUCUUGAU
si-PLK1-R-3	CAAGAAGAAUGAAUACAGUAU

Table S2. Primer sequence

Name	Sequence (5'–3')
H-GAPDH-F	AACGGATTTGGTCGTATTGGGCGC
H-GAPDH-R	TCCTGGAAGATGGTGATGGGATTT
H-PLK1-F	GTCGTAGGATTCCACGGCTTTTTC
H-PLK1-R	TTCACCTCCAGATCTTCATTCAGG
H-AURKB-F	CACAGAGACATAAAGCCAGAAAAT
H-AURKB-R	CCACCAGCAGCTCATAGCAAAGCA
H-CDK1-F	CAGACTAGAAAGTGAAGAGGAAGG
H-CDK1-R	ATGGAAAGAAACTCAAAGATGAGA
H-FYN-F	CCCCAACTACAACAACTTCCACGC
H-FYN-R	CTTCCCACCAATCTCCTTCCGAGC

Table S3. The top 15 differentially expressed genes in the GSE38264 dataset

Name	Description	log2FoldChange	*p* val	up/down
CSGALNACT1	chondroitin sulfate N-acetylgalactosaminyltransferase 1	1.98	6.97E-09	up
RUNX1T1	RUNX1 translocation partner 1	1.98	7.4E-09	up
BNC2	basonuclin 2	1.97	8.14E-09	up
ZFPM2	zinc finger protein, FOG family member 2	1.96	9.39E-09	up
ZNF521	zinc finger protein 521	1.96	9.8E-09	up
COL6A1	collagen type VI alpha 1 chain	1.95	1.07E-08	up
SFRP2	secreted frizzled related protein 2	1.95	1.16E-08	up
TENM3	teneurin transmembrane protein 3	1.95	1.2E-08	up
CLMP	CXADR like membrane protein	1.94	1.27E-08	up
COL6A2	collagen type VI alpha 2 chain	1.94	1.28E-08	up
NTRK3	neurotrophic receptor tyrosine kinase 3	1.94	1.34E-08	up
FGF7	fibroblast growth factor 7	1.94	1.36E-08	up
DDR2	discoidin domain receptor tyrosine kinase 2	1.94	1.39E-08	up
ANKRD29	ankyrin repeat domain 29	1.94	1.44E-08	up
SRPX	sushi repeat containing protein, X-linked	1.93	1.5E-08	up
KIF25-AS1	KIF25 antisense RNA 1	-1.00	0.00342	down
CXorf40B	chromosome X open reading frame 40B	-1.00	0.00342	down
ULBP2	UL16 binding protein 2	-1.00	0.00341	down
TMEM51-AS1	TMEM51 antisense RNA 1	-1.00	0.00341	down
GOLGA3	golgin A3	-1.00	0.00339	down
RAB11FIP3	RAB11 family interacting protein 3	-1.00	0.00339	down
SEH1L	SEH1 like nucleoporin	-1.00	0.00339	down
MARK4	microtubule affinity regulating kinase 4	-1.00	0.00338	down
RNF5P1///RNF5	ring finger protein 5 pseudogene 1///ring finger protein 5	-1.00	0.00338	down
RNF5P1///RNF5	ring finger protein 5 pseudogene 1///ring finger protein 5	-1.00	0.00338	down
C19orf70	chromosome 19 open reading frame 70	-1.00	0.00338	down
YTHDF1	YTH N6-methyladenosine RNA binding protein 1	-1.00	0.00338	down
MTMR3	myotubularin related protein 3	-1.00	0.00338	down
FZD5	frizzled class receptor 5	-1.00	0.00337	down
SIPA1L3	signal induced proliferation associated 1 like 3	-1.00	0.00337	down

Table S4. The top 15 differentially expressed genes in the GSE130598 dataset

Name	log2FoldChange	*p* val	up/down
NEK2	3.78	6.25E-21	up
TTK	3.84	5.8E-19	up
AURKB	4.35	9.83E-19	up
CDK1	4.33	1.47E-18	up
BUB1	3.36	1.23E-17	up
PLK1	3.86	4.59E-17	up
PLK4	2.76	5.62E-17	up
AURKA	2.74	9.56E-16	up
BUB1B	3.58	1.31E-14	up
PKMYT1	2.87	5.88E-14	up
PBK	2.73	1.62E-11	up
CHEK1	2.59	1.95E-11	up
CIT	2.17	2.93E-10	up
GSG2	1.71	7.28E-08	up
MAPK13	3	2.47E-07	up
MYLK	-6.68	6.62E-20	down
HSPB8	-6.07	1.61E-15	down
PDK4	-5.26	4.08E-14	down
EPHA3	-3.37	7.85E-13	down
PRKG1	-3.7	2.11E-12	down
NPR1	-2.95	2.36E-12	down
ROR1	-3.47	7.07E-12	down
EPHA7	-3.71	6.29E-11	down
FGFR1	-3.36	1.45E-10	down
PKDCC	-4.24	2.19E-10	down
NTRK2	-2.86	5.38E-10	down
NEK7	-1.57	7.33E-10	down
DCLK1	-2.57	1.22E-09	down
GRK5	-2.2	2.39E-09	down
SPEG	-3.46	3.92E-09	down